Original Article

Avicenna Journal of Medical Biotechnology
Volume 17, Issue 3, 186-195
https://doi.org/10.18502/ajmb.v17i3.19277

Check for updates

The Quality and Quantity of Nanoparticles Extracted from Human Adipose Tissue Derived-Mesenchymal Stem Cells

Mobina Karimi [1], Banafsheh Heidari [2*], Hanieh Jafary [1] and Kavosh Zandsalimi [3]

1. Department of Biology, SR.C, Islamic Azad University, Tehran, Iran
2. Department of Regenerative Medicine and Biotechnology in Wound Healing, Medical Laser Research Center, Yara Institute, ACECR, Tehran, Iran
3. Department of Medical Laser (MLRC), Medical Laser Research Center, Yara Institute, ACECR, Tehran, Iran

Abstract

Background: Nanoparticles, as small extracellular vesicles, are considered promising tools in tissue engineering and regenerative medicine. This study aimed to investigate the effects of different processing and culture condition on the quality and quantity of extracts derived from human Adipose-Mesenchymal Stem Cells (AD-MSCs).

Methods: AD-MSCs were proliferated in both the experimental and control groups. Nanoparticles were extracted from AD-MSCs-extracts and analyzed using SEM, TEM, DLS, Zeta potential, FTIR and BCA analyses. The morphological characteristics (shape, size, distribution, surface topography, and agglomeration/aggregation), structural appearance (poly-disperse intensity, colloidal particle behavior, surface charge, and stability), chemical properties (functional groups and ionic interactions) and total protein concentration were detected in the extracted nanoparticles. Additionally, the morphological characteristics, apoptosis, mitochondrial oxidoreductase activity, and migration potential of AD-MSCs in both groups were evaluated using acridine orange staining, MTT, and scratch assays.

Results: In the experimental group, 100% of the nanoparticles had a diameter of 112.8± 25 *nm*, with the most frequency of 111.4 *nm*. However, in the control group, 72% of nanoparticles had a diameter of 350.2±43.6 *nm* with the highest frequency of 339.8 *nm* ($p \leq 0.05$). The Z-average, Poly-disperse intensity, and electrostatic stability of nanoparticles in the control and experimental groups were 171.9 *nm*, 0.727 and -0.000011 cm^2/Vs *vs.* 103.7 *nm*, 0.205 and 0.000481 cm^2/Vs, respectively ($p \leq 0.05$). In the experimental group, Zeta potential was -61.8 *mV*, which is in the range of $\zeta > -30mV$. Although, Zeta potential in the control group was -1.5 *mV*, which is in the range of $-30\ mV < \zeta < 30\ mV$ ($p \leq 0.05$). Total protein concentrations in the control and experimental groups were 11 and 41%, respectively ($p \leq 0.05$).

Conclusion: Nanoparticles derived from AD-MSCs have high therapeutic applications in tissue engineering and regenerative medicine.

*** Corresponding author:**
Banafsheh Heidari, Ph.D.,
Department of Regenerative Medicine and Biotechnology in Wound Healing, Medical Laser Research Center, Yara Institute, ACECR, Tehran, Iran
E-mail:
b.heidari@acecr.ac.ir,
b.heidari@acecr.ac.ir
Received: 15 Feb 2025
Accepted: 19 May 2025

Keywords: Acridine orange, Control groups, Fourier transform infrared, Immunologic factors, Nanoparticles, Obesity, Regenerative medicine, Spectroscopy, Static electricity, Tissue engineering

To cite this article: Karimi M, Heidari B, Jafary H, Zandsalimi K. The Quality and Quantity of Nanoparticles Extracted from Human Adipose Tissue Derived-Mesenchymal Stem Cells. Avicenna J Med Biotech 2025;17(3):186-195.

Introduction

Cell-free therapy has been widely used in treating various diseases, including immunological and neurological disorders, degenerative diseases, liver failure (fibrosis, cirrhosis, and ischemia-reperfusion injury), cardiovascular diseases (myocardial infarction and ischemia), renal disorders, pulmonary deficiencies, and skin injuries. Cell derivatives not only have numerous clinical applications in treating various diseases but are also used as biomarkers for early rapid diagnosis of abnormalities/diseases. There are several studies demonstrated that the paracrine factors secreted by various cell types are specialized and unique in their types,

concentration of biologically active compounds and functional properties. Therefore, the identification of these factors can specifically identify the type of cells (cancer cells or normal cells) and their functional nature, aiding in their early diagnosis and targeted treatment [1-4].

The bioactive paracrine factors in cell derivatives regulate many biological and pathological processes; such as establishing intercellular communication, altering/modifying cell signaling, and inducing the pathways related to immune responses, inflammation, differentiation, metastasis, migration, angiogenesis, apoptosis, *etc.* [5-7]. One of the most important bioactive components in cell derivatives is exosomes with a diameter of 40-160 *nm* and a density of 1.13-1.19 *g/ml*. These microvesicles have a phospholipid bilayer membrane and contain various biological compounds such as lipids, DNA, mRNA, miRNA, various types of proteins such as heat shock proteins (HSP70 and Hsp90), enzymes, membrane transporters (Annexin and GTPases), and tetraspanins (CD9, CD63, CD81, and CD82). Exosomes are non-toxic, biocompatible, and biodegradable. They can transfer from the blood-brain barrier or blood-testicular barrier and exert therapeutic effects on the CNS and gametes.

In addition, they can specifically bind to the target cells due to their surface receptors. The other advantages of exosomes include high stability in biological fluids, strong immunomodulatory properties, long-term storage capability without the need for various cryoprotectants, and the potential to engineer them for specific purposes such as producing synthetic exosomes [1,4,5,8,9]. Another advantage of exosomes is their portability, affordable and ease of trans-port, which eliminates the need for specialized carriers or special laboratory-medical preparations. These therapeutic nanoparticles can be efficiently frozen at -80°*C* with or without non-penetrating cryoprotectants such as trehalose or sucrose and thawed at 37°*C* while maintaining the therapeutic efficacy. This allows exosome therapy to expedite treatment for acute diseases requiring immediate intervention such as cerebral ischemia, myocardial infarction, or other rapidly progressive diseases because the frozen exosomes can immediately be thawed and injected into the patient. In contrast, cell therapy requires cells to be cultured and reactivated post-thaw, along with viability assessment before transplantation [4,5,8-10].

Exosomes are divided into three groups based on size heterogeneity, including ExoA, ExoB, and ExoC. ExoA has dimensions of 40-75 *nm*, ExoB has a size of 75-100 *nm*, and ExoC has a size of 100-160 *nm* [5,11]. Based on their content heterogeneity, exosomes are categorized into three groups, including Exo 1, Exo 2, and Exo 3. The first group, Exo 1, contains CD63 molecular marker and protein content of "X". Exo 2 has CD9 biomolecular, nucleic acids and protein content of "Y". Exo 3 includes CD81 molecular marker and protein content of "Z" [5,11,12]. In terms of functional heterogeneity, exosomes are also divided into three groups: Exo α, Exo β, and Exo γ. Exo α imparts pro-survival signals on recipient cells. Exo β modulates the apoptotic process and Exo γ imparts immunomodulation on recipient cells [5,11-13].

This study aimed to investigate the effect of culture conditions and processing on the quality and quantity of nanoparticles isolated from human Adipose-Mesenchymal Stem Cells (AD-MSCs). For this purpose, the effect of different culture conditions on the morphological characteristics (shape, size, distribution, surface topography, and agglomeration/aggregation), structural appearance (poly-disperse intensity, colloidal particle behavior, surface charge, and stability), chemical properties (functional groups and ionic interactions) and total protein concentration of nanoparticle in the cell extracts using SEM, TEM, DLS, Zeta potential, FTIR, and BCA analyses were examined. Additionally, the cell count, apoptosis, mitochondrial oxidoreductase activity, and migration potential of AD-MSCs were detected using microscopic examination, acridine orange staining, MTT, and scratch assay.

Materials and Methods

The study was approved by the Research Ethics Committee of the Islamic Azad University, Science and Research Unit, Tehran (IR.IAU.SRB.REC.1403.082). Human adipose tissue (lipoaspirate) was obtained from healthy donors according to inclusion criteria. Donor inclusion criteria included age 45 and 55 years, no drug addiction, metabolic diseases, and liver disorders, as well as, absence of viral (HIV-1/2 Ab, HBV, HCV, syphilis and HPLV), mycoplasma, fungal, and bacterial infections. Except where otherwise indicated, all chemicals were obtained from Sigma-Aldrich (St. Louis, MO, USA).

Collection of adipose tissue and its macroscopic and microscopic evaluations

Following liposuction of abdominal fat tissue using 4 *mm* cannulas, the adipose tissues were transferred to the laboratory on ice (4°*C*) for 20 *min*. The samples were prepared and evaluated using a protocol previously described by Heidari *et al* [14,15] with minor modifications. In the macroscopic evaluation, adipose tissues were examined for color, volume, density, and the presence of hematoma, hemorrhage, contusion, cysts and any abnormality. For histomorphological evaluation, 2 *mg* of adipose tissue was sent to the pathology laboratory in 25 *ml* of 10% formalin. Three paraffin blocks were prepared and 30 histological glass slides, each 5 *μm* thick, were prepared from paraffin blocks using a microtome (10 glass slides/paraffin block). Any evidence of necrosis, cysts, inflammatory cell invasion, calcification, fibrosis, cell rupture and ECM disintegration were detected using H&E staining. Each slide was evaluated separately by two blind pathologists and at least 5 fields were examined per slide.

Isolation and validation of mesenchymal stem cells derived from adipose tissue

After macroscopic and microscopic evaluations, adipose tissues were washed three times with warm Phosphate Buffered Saline (PBS) containing 100 *U/ml* penicillin, and 100 *mg/ml* streptomycin at 1200 *rpm* for 10 *min*. Then, the tissues were digested by a two-step enzymatic digestion method using collagenase type I (1 *mg/ml*) and trypsin-EDTA (0.25/1 *mM*) for 45 *min* at 37°*C*. The digested suspension was filtered through 70 *µm* nylon mesh and centrifuged at 1200 *rpm* for 10 *min*. Cell suspension was cultured in DMEM/F12 medium containing 100 *IU* Penicillin, 10% FBS and 100 *µg/ml* of streptomycin in an incubator at 37°*C*, 80% humidity and 5% CO_2 for 3-5 days. After 70-80% confluency, the attached cells were trypsinized using trypsin-EDTA and cultured in the same condition at 37°*C*, 80% humidity and 5% CO_2 (Passage 1). In the study, adipose tissue-derived MSCs were passaged 3 times and confirmed using flow cytometry, which confirmed the expression of CD29, CD14, CD45, CD34, CD105, and CD44 markers. At last, the confirmed AD-MSCs in passage 4 were frozen at a density of 9×10^5 cells in cryovials containing freezing medium (50% DMEM, 10% DMSO, 40% FBS) at -196°*C*.

Study design

The frozen AD-MSCs were thawed at 37°*C* and propagated at a cell density of 5×10^6 *cells/ml* in DMEM/F12 culture medium composed of 10% FBS, 100 *mg/ml* streptomycin and 100 *U/ml* penicillin at 37°*C*, 80% humidity and 5% CO_2. The adherent elongated MSCs displayed a homogeneous fibroblast-like morphology with spindle or triangular-shaped cell bodies, and large elliptical nuclei. The nonadherent cells were removed after 12 *hr* during the medium change. Then, the 25 cm^2 culture flasks were divided randomly into two groups, including the control and experimental groups.

Extraction of nanoparticles in different groups

AD-MSCs in the experimental groups were incubated in DMEM/F12 composed of 10% KnockOut serum (Exo-free serum), 100 *mg/ml* streptomycin and 100 *U/ml* penicillin at 37°*C*, 22% O_2, and 5% CO_2 for 48 *hr*. Then, the supernatant was collected and centrifuged at 300 *g*, 2000 *g*, and 10000 *g* for 10 *min*, 10 *min*, and 30 *min*, respectively. The extracted media were passed through a 0.22 *µm* nylon mesh and centrifuged twice at 100000 *g* for 70 *min*. The pellet was processed in 400 *µl* PBS and stored at -80°*C* until use. In the control group, AD-MSCs were propagated with fresh culture medium containing DMEM/F12, 10% FBS, 100 *mg/ml* streptomycin and 100 *U/ml* penicillin for 48 *hr* in an atmosphere of 5% CO_2, 37°*C*, and 22% O_2. After 48 *hr*, the supernatant were collected and centrifuged at 300 *g*, 2000 *g*, and 10000 *g* for 10 *min*, 10 *min*, and 30 *min*, respectively. The extracted media were passed through a 0.22 *µm* nylon mesh and stored at -80°*C* until use.

The impact of culture condition on AD-MSC characteristics

The study evaluated how culture conditions affect the apoptosis, migration, and viability rate of AD-MSCs. To evaluate apoptosis using acridine orange staining, AD-MSCs were suspended at a density of 5×10^5 cells/well in a 6-well culture plate. In the experimental group, the cells were incubated in a culture medium composed of 1% KnockOut serum (Exo-free serum), 100 *mg/ml* streptomycin, and 100 *U/ml* penicillin at 37°*C*, 5% CO_2, 5% O_2, and 80% humidity for 24 *hr*. The control group received DMEM/F12 supplemented with 10% FBS, 100 *IU*/ml penicillin, 100 *µg/ml* streptomycin at 37°*C*, 5% CO_2, 22% O_2, and 80% humidity for 24 *hr*. Then, 100 *µl* acridine Orange diluted in 100 *ml* of PBS was added to each well for 10 *min* at 37°*C* in the dark. After this time, the plates were washed twice with PBS and examined using a fluorescence microscope.

To investigate the migration of AD-MSCs, the scratch test was performed in both the control and experimental groups. For this purpose, AD-MSCs were cultured at a density of 5×10^5 cells/well in a 6-well culture plate using a medium with 1% KnockOut serum in the experimental group and 10% FBS in the control group for 24 *hr*. After 80-90% confluency, the scratch was created in the cell monolayer with a yellow pipette tip (10-100 *µl*). Images were captured immediately (0 *hr*), 6 *hr*, 12 *hr*, 18 *hr*, and 24 *hr* post-scratch and analyzed using ImageJ software.

The mitochondrial oxidoreductase activities of AD-MSCs in both the control and experimental groups using MTT assays were investigated. Approximately, 1×10^4 AD-MSC were propagated under different conditions in each well in 96 well plates and incubated for 24 *hr*. Then, 100 *µl* MTT solution (0.5 *mg/ml*) was added to each well for 3 *hr* in the dark. MTT solution was carefully aspirated and 100 *µl* DMSO was added to dissolve the formazan precipitate. The absorbance was detected at 570 *nm* in a plate reader.

The effect of culture condition on the adipose tissue-derived MSCs-nanoparticles

To characterization of nanoparticles extracted from AD-MSCs, the morphological characteristics (shape, size, distribution, surface topography, and agglomeration/aggregation), structural appearance (poly-disperse intensity, colloidal particle behavior, surface charge, and stability), chemical properties (functional groups and ionic interactions) and total protein concentration of nanoparticle in different culture conditions using SEM, TEM, DLS, Zeta potential, FTIR, and BCA analyses were evaluated.

Morphological characteristics of nanoparticles in different conditions

Shape, size, distribution, surface topography, and agglomeration/aggregation of nanoparticles in both the control and experimental groups were detected using SEM and TEM. To SEM analysis, the extracted nanoparticles were fixed with paraformaldehyde 2% and

diluted with distilled water. Then, 5 μl exosomes were transferred onto silicon chips and placed in acetone for one *min* to dehydrate and dry. After washing and drying, the nanoparticles were analyzed by an electron microscope at a voltage of 30 *KV*. For TEM evaluation, the nanoparticles from different groups were fixed using glutaraldehyde 1%. The drop was placed on a carbon-coated grid and dried for 2 *min* at room temperature. Then, the slides were washed twice with sterile PBS and stained with uranyl acetate 1% for 16 *min*. The corresponding images in both groups were recorded using a Philips CM-120 microscope (made in the Netherlands) with a voltage of 120 *KV*.

Structural appearance of nanoparticles extracted from the control and experimental conditions

Structural characteristics of nanoparticles including poly-disperse intensity, colloidal particle behavior, Z-average, surface charge, and stability in both the control and experimental groups were detected using DLS and Zeta potential analysis. For this purpose, 100 μl of extracted nanoparticles in different groups were mixed with 400 μl of filtered PBS (1:5 ratio) and sonicated on ice for 20 *min*. Then, the sample was placed in a SZ-100 device (Horiba Company, Japan) and a graph related to the nanoparticles was recorded along with the zeta potential (surface charge present in the nanoparticles and their electrostatic stability).

Chemical properties of extracts from AD-MSCs in the control and experimental conditions

FTIR analysis revealed the functional groups and chemical composition of extracts through their infrared absorption. Spectral investigation of nanoparticles in the extracts was obtained at 4000-4000 cm^{-1} using an AVATAR spectrometer (Thermo, USA). This analysis determined the biochemical composition of extracts, highlighting the similarities and differences in the molecular structure between the control and experimental groups.

Total protein concentration in the extracts from AD-MSCs

Total protein concentration was evaluated using a BCA protein assay kit (Thermo Scientific Pierce, Rockford, IL, USA). For this purpose, various volumes of the nanoparticles extracts (10, 20, 30, 40, and 80 *ml*) were centrifuged to collect samples with increasing nanoparticles doses. The protein in the samples were released using a specific protocol, and isolated nanoparticles were re-suspended in 200 μl of RIPA buffer containing a protease inhibitors cocktail, followed by sonication for 5 *min*. BSA standard and samples (25 μl) were transferred to a 96-well plate and working reagent (200 μl) was added to each well (in a 50:1 ratio of assay reagents A and B). The plate was incubated at 37°*C* for 30 *min*, before being analyzed with a spectrophotometer at 562 *nm* (Victor3, Perkin-Elmer, and Waltham, MA, USA).

Statistical analysis

The statistical software used in this study was SPSS 16 and GraphPad Prism 6. Quantitative data will be presented as mean and standard deviation (in case of non-normality from the mean and range) and qualitative data will be presented as frequency and percentage. T-tests and Wilcoxon tests will be used to compare the results between groups. A statistical significance level more than or equal to 0.05 is considered.

Results

Proliferation and differentiation of AD-MSCs in different culture conditions

The microscopic evaluation of AD-MSCs in different groups is shown in figure 1. These cells were observed to be spindle-shaped (fibroblast-like) with fully extended invasion. Total concentration of AD-MSCs reached to 20, 30, 45, 60, 80 and 100% on days 1, 2, 3, 4, 5 and 6, respectively (Figure 1). The expression of CD29, CD14, CD45, CD34, CD105, and CD44 molecular markers on AD-MSCs are demonstrated in figure 2. AD-MSCs propagated in the control and experimental groups were able to differentiate into chondrocytes (metachromatic violet), osteocytes (reddish-brown calcium deposits) and adipocytes (yellow-orange fatty vacuoles) (Figure 3). There were no significant differences in the total counts, differentiation capacity, and migration of AD-MSCs between the control and experimental groups (Figures 3 and 4; $p>0.05$).

Effect of culture conditions on the mitochondrial reductase activity and apoptosis and of AD-MSCs

The apoptotic rate of AD-MSCs in the control and experimental groups is shown in figures 5A, and 5B. According to the acridine orange staining, AD-MSCs demonstrated green fluorescent dyes, indicating no apoptosis of AD-MSCs in different groups. No statistically significant difference was observed in the mitochondrial reductase activities of AD-MSCs between the control (97.5%) and experimental (95.9%) groups (Figure 5C; $p>0.05$).

Size, shape and surface topography of extracted nanoparticles in different culture conditions

The morphological characteristics of nanoparticles derived from AD-MSCs are demonstrated in figure 6 and Histogram 1. Nanoparticles in the different groups are observed as spherical bodies with a uniform and consistent distribution using SEM. There was a statisti-

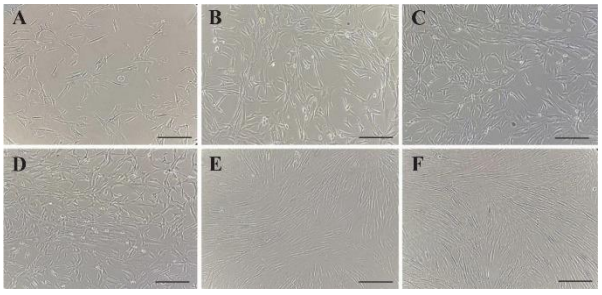

Figure 1. Proliferation of AD-MSCs at passage 3 on days 1 (A), 2 (B), 3 (C), 4 (D), 5 (E) and 6 (F) post culture initiation, magnification 40 *X*.

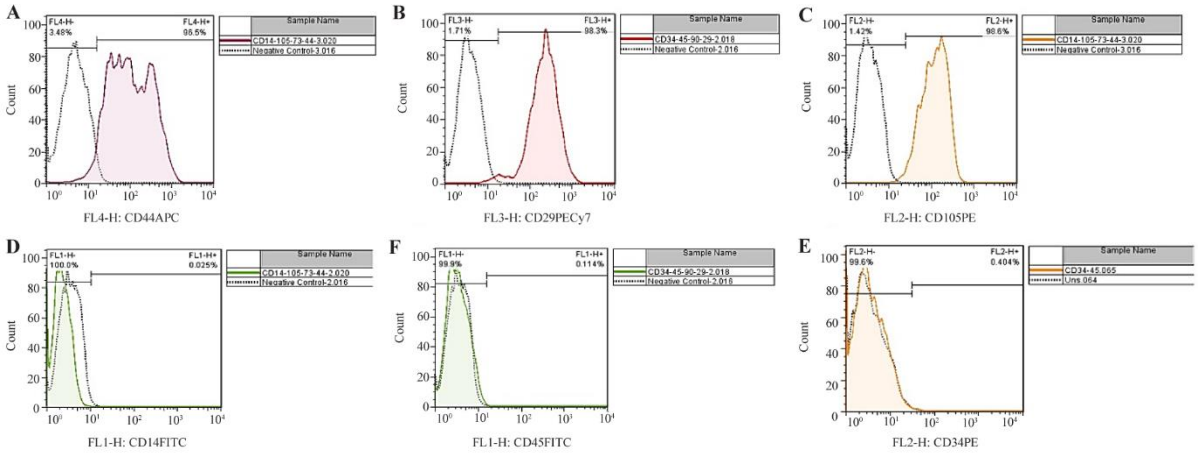

Figure 2. The expression of CD44 (A), CD29 (B), CD105 (C), CD14 (D), CD45 (E), and CD34 (F) biomarkers on AD-MSCs.

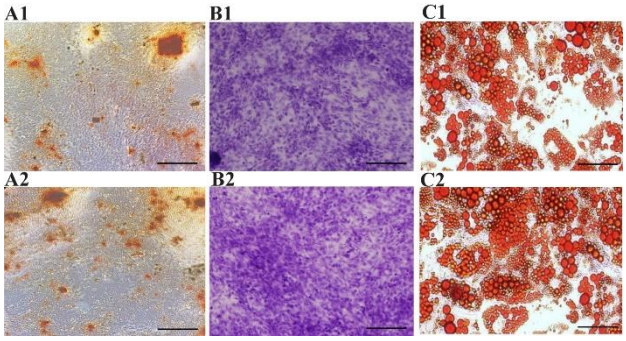

Figure 3. Differential potentials of AD-MSCs into osteocytes (A1, A2), chondrocytes (B1, B2) and adipocytes (C1, C2) in the control (A1-C1) and experimental (A2-C2) groups, magnification 40*X*.

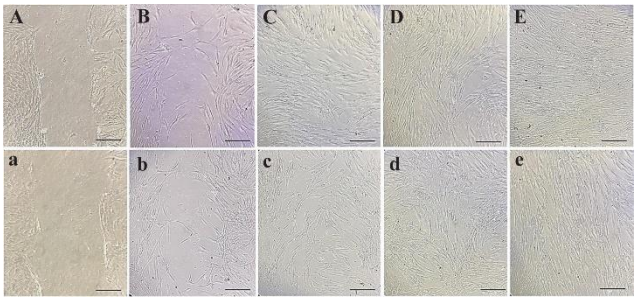

Figure 4. Migration of AD-MSCs at 0 *hr* (A, a), 6 *hr* (B, b), 12 *hr* (C, c), 18 *hr* (D, d) and 24 *hr* (E, e) in the control (A-E) and experimental (a-e) groups, magnification 40*X*.

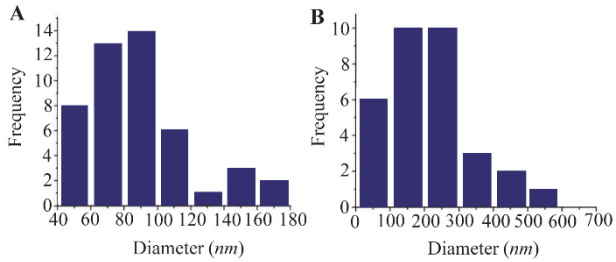

Histogram 1. Frequency and distribution of nanoparticles in the experimental (A) and control (B) groups.

cal difference in the size of extracted nanoparticles in the control and experimental groups ($p \leq 0.05$). In the control group, the greatest number of nanoparticles was in the range of 100-300 *nm*, while in the experimental group, the highest frequency of nanoparticles was in the range of 60-100 *nm* ($p \leq 0.05$). SEM showed that the extracted nanoparticles in the experimental group were in the range of exosomes (40-160 *nm*), while most nano-particles in the control group were in the range of micro-vesicles or ectosomes (200-1000 *nm*) (Figure 6; Histogram 1; $p \leq 0.05$).

Aggregation and dispersion of extracted nanoparticles in different culture conditions

The effect of culture conditions on the structure

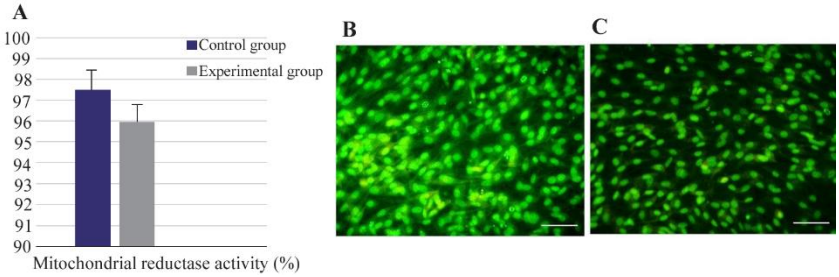

Figure 5. Mitochondrial reductase activities (A), and apoptosis of AD-MSCs in the control (B) and experimental (C) conditions with a magnification of 40*X*.

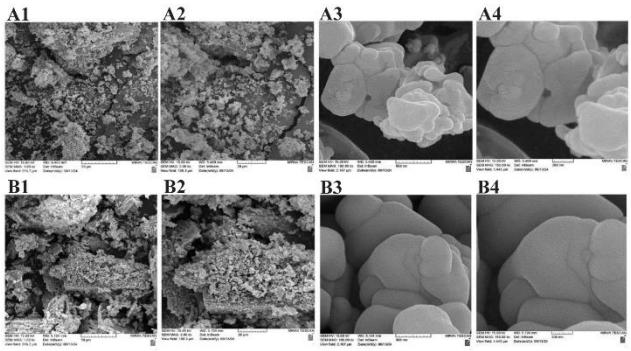

Figure 6. Extracted nanoparticles in the experimental (A1-4) and control (B1-4) groups with magnifications of 50 μm (A1, B1), 20 μm (A2, B2), 500 *nm* (A3, B3) and 200 *nm* (A4, B4).

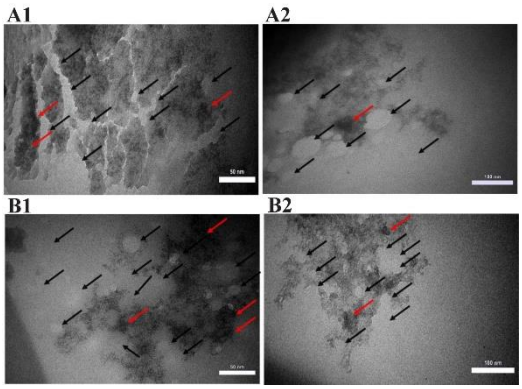

Figure 7. Aggregation, dispersion, and agglomeration of extracted nanoparticles in the control (A) and experimental (B) groups with magnifications of 50 *nm* (A1, B1) and 100 *nm* (A2, B2). Black arrows demonstrate the typical nanoparticles and red arrows are agglomerated and aggregated nanoparticles.

characteristics and dispersion/aggregation of nanoparticles from AD-MSCs is shown in figure 7. In the control group, the variation in size and dispersion of nanoparticles is demonstrated using TEM analysis. The most dispersion and aggregation of nanoparticles are in the control group, while this amount is significantly lower in the experimental group ($p \leq 0.05$; Figure 7). Also, the agglomeration of nanoparticles in the control group was significantly higher than that of experimental group (Figure 7; $p \leq 0.05$).

Zeta potential and electrostatic stability of nanoparticles in different culture conditions

The Zeta potential and electrostatic stability of nanoparticles in both the control and experimental groups are shown in Figure 8. Zeta potential curves in the control and experimental groups have a narrow peak, indicating that the surface charges of nanoparticles are uniform. There are statistically significant differences in the Zeta potential and electrostatic stability of nanoparticles between the control and experimental groups ($p \leq 0.05$). In the experimental group, Zeta potential was -61.8 *mV*, which is in the range of $\zeta > -30$ *mV*, so the nanoparticles were stable. On the other hand, the Zeta potential in the control group was -1.5 *mV*, which is in the range of $-30\ mV < \zeta < 30\ mV$ ($p \leq 0.05$). So, the particles were unstable and tended to aggregate (Figure 8). In addition, the electrostatic stability of nanoparticles in the control and experimental groups are -0.000011 cm^2/Vs and 0.000481 cm^2/Vs, respectively ($p \leq 0.05$).

Poly-disperse intensity and Z-Average of nanoparticles in different groups

A statistically significant difference is observed in the Poly-disperse Intensity (PI), dimensions, and Z-average of nanoparticles between the control and experimental groups (Figure 9; $p \leq 0.05$). According to figure 9, in the experimental group, 100% of the nanoparticles had a diameter of 112.8±25 *nm*, with the most frequency of 111.4 *nm*. However, in the control group, 28% of the nanoparticles had a diameter of 35.6±3.2 *nm* with the highest frequency of 35.7 *nm*, and the remaining 72% of nanoparticles had a diameter of 350.2± 43.6 *nm* with the highest frequency of 339.8 *nm* ($p \leq 0.05$; Figure 9). The PI and Z-average of nanoparticles in the control and experimental groups are 171.9 *nm* and 0.727 *vs.* 103.7 *nm* and 0.205, respectively (Figure 9).

A

Calculation results		
Peak No.	**Zeta potential**	**Electrophoretic mobility**
1	-1.5 *mV*	-0.000011 cm^2/vs
2	… *mV*	… cm^2/vs
3	… *mV*	… cm^2/vs

Zeta potential (Mean): -1.5 *mV*
Electrophoretic mobility mean: -0.000011 cm^2/vs

B

Calculation results		
Peak No.	**Zeta potential**	**Electrophoretic mobility**
1	-61.8 *mV*	-0.000481 cm^2/vs
2	… *mV*	… cm^2/vs
3	… *mV*	… cm^2/vs

Zeta potential (Mean): -61.8 *mV*
Electrophoretic mobility mean: -0.000481 cm^2/vs

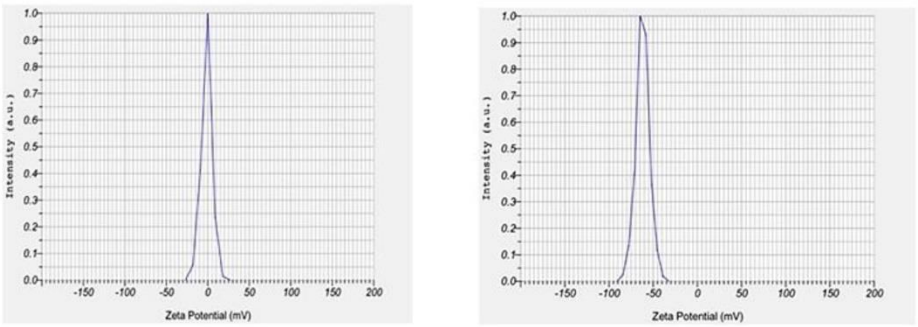

Figure 8. Zeta potential and electrostatic stability of nanoparticles extracted from AD-MSCs in the control group (A) and experimental group (B).

A

Calculation results				
Peak no.	S.P. Area ratio	Mean	S.D.	Mode
1	0.28	35.6 *nm*	3.2 *nm*	35.7 *nm*
2	0.72	350.2 *nm*	43.6 *nm*	339.8 *nm*
3	-	-	-	-
Total	1.00	260.9 *nm*	146.5 *nm*	339.8 *nm*

Cumulant operations
Z-average: 171.9 *nm*
PI: 0.727

B

Calculation results				
Peak no.	S.P. Area ratio	Mean	S.D.	Mode
1	1.00	112.8 *nm*	25.0 *nm*	111.4 *nm*
2	-	-	-	-
3	-	-	-	-
Total	1.00	112.8 *nm*	25.0 *nm*	111.4 *nm*

Cumulant operations
Z-average: 103.7 *nm*
PI: 0.205

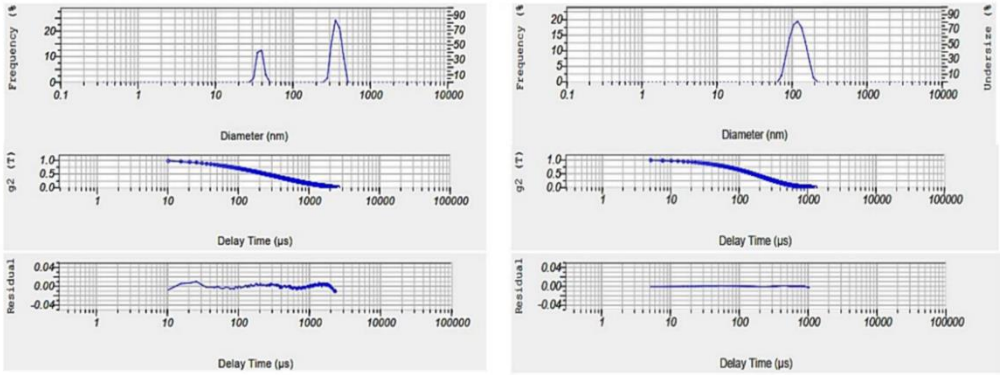

Figure 9. Poly-disperse intensity and Z-average of nanoparticles extracted from AD-MSCs in the control group (A) and experimental group (B).

Chemical properties and functional groups of extracts in the control and experimental conditions

The chemical composition and functional groups of nanoparticles extracted in the control and experimental conditions are shown in figure 10. There was no significant difference in the peaks, wavelengths, and their interpretations between the control and experimental groups ($p>0.05$). The peaks, wavelengths, and their interpretations, particularly the relevant functional groups, are detailed in Figure 10. FTIR analysis indicates that the extracted nanoparticles contain various compounds, including proteins (according to amide I and II peaks), lipids (due to aliphatic C-H peaks), glycoproteins or phospholipids (according to C-O or P-O peaks), and nucleic acids (due to the presence of P-O peak) (Figure 10).

Total protein concentration in the extract derived from AD-MSCs

The absorption rate of standard solutions and total protein contents in the control and experimental groups are demonstrated in figure 11. There was a statistical significant difference in the total protein concentration between the control and experimental groups ($p\leq0.05$). The amount of total protein in the experimental and

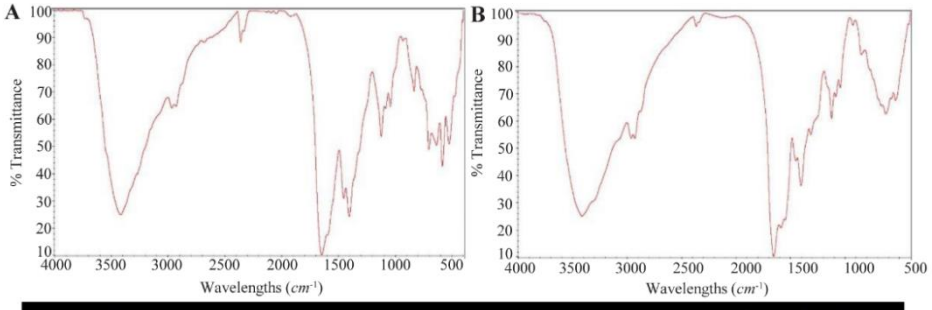

Functional groups	Bond	Wavelength (cm^{-1})
Alcohols, Amines, and Amides	O-H stretching bond and N-H stretching bond	**3413**
Methylene groups (CH_2) in aliphatic chains	C-H asymmetric stretching bond	**2930**
CO_2	C≡N asymmetric stretching bond	**2364**
Amide I in Proteins	C=O stretching bond	**1654**
Amide II in Proteins	N-H Bending bond and C-N stretching bond	**1544**
Carboxylates	COO- symmetric stretching bond	**1403**
Alcohols, Ethers, Esters, or Phosphates	C-O-C stretching bond or PO_2^- stretching bond	**1122**
Aromatic cycles	C-S, C-C out of plane bending bond	**623**
Halides or disulfide bonding	P-O stretching bond	**530**

Figure 10. The functional groups, wavelengths, and their interpretations in the extracts of the control (A) and experimental (B) conditions using FTIR analysis.

sample	blank s	Experimental group	Control group
a1	1.1912	1.2347	1.3364
a2		1.2175	1.3237
a3	1.1884	1.2252	1.3243
Average	1.1898	1.2258	1.328133
Absorption	0	0.036	0.138333
Concentration (1/5)		0.231391	0.821889
Final Concentration		1.156953	4.109444
Total protein concentration rate (%)		41.09444	11.56953

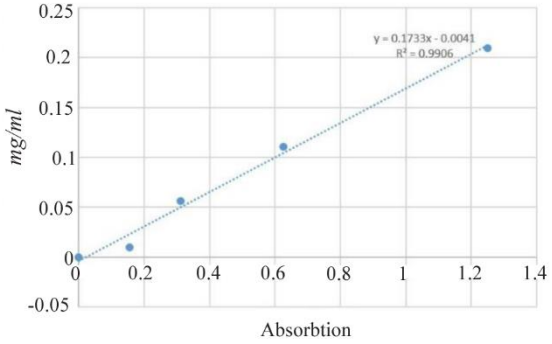

Figure 11. Absorption rate and total protein concentrations of AD-MSCs extracts in different groups.

control groups are measured as 41.09444, and 11.56953%, respectively (Figure 11).

Discussion

In the present study, nanoparticles with a diameter of 112.8±25 *nm* (mode: 111.4 *nm*) were achieved in the experimental group. The PI, Z-average, and Zeta potential of nanoparticles were 103.7 *nm*, 0.205, and -61.8 *mV*, respectively. In addition, the electrostatic stability of nanoparticles derived from AD-MSCs was 0.000481 cm^2/Vs, Consistent with our results, Safwani and his colleagues in 2016 evaluated the effect of different culture conditions on propagation of MSCs derived from adipose tissue.

This study aimed to introduce the alternative culture conditions that provide a better and safer environment for cell growth. They divided AD-MSCs into four experimental groups including:
1) 21% oxygen with FBS, 2) 21% oxygen without FBS, 3) 2% oxygen with FBS and 4) 2% oxygen without FBS. Microscopic examination showed that the AD-MSCs in all experimental conditions had spindle-shaped and fibroblast-like morphology. They expressed the positive molecular markers such as CD105, CD73, CD90 and CD44 more than 90% of cells. However, the hematopoietic cell biomarkers including CD34, CD19, CD14 and CD45 do not express on the cell surface. They presented a significant increase in the expression of CD14 and CD34 in the cells cultured in the serum starvation group with 2% oxygen [16]. Kim *et al* in 2021 evaluated the nanoparticles extracted from human umbilical cord-MSCs. They also investigated the expression of pro-inflammatory factors in the cell extracts depending on the cellular status.

Additionally, the wound healing process and angiogenesis activities were investigated using nanoparticles extracted from a human umbilical cord-MSCs. Human umbilical cord-MSCs were randomly divided into two the control and experimental groups. In the control group, MSCs were cultured in a low-glucose medium supplemented with 10% FBS and 1% antibiotic-antifungal in a humidified incubator with 5% CO_2 at 37°*C*. However, the cells in the experimental group propagated in a medium containing 1% antibiotic-antifungal mixture under serum starvation conditions. The expression of CD63 and CD81 biomarkers in the nanoparticles extracted from umbilical cord-MSCs were examined using Western Blot analysis. In this study, FTIR analysis revealed an amide I absorption band at 1650 cm^{-1}, an amide II absorption band at around 1540 cm^{-1}, an absorption for the lipid acyl chain between 2860 cm^{-1} and 2940 cm^{-1}, and an absorption of the carbonyl ester group around 1740 cm^{-1}, which are directly related to all subpopulations of exosome. The expression of HGF and bFGF increased in the control group compared to the experimental group. Also, the release of pro-inflammatory cytokines was significantly reduced in the control condition compared to the experimental group [17]. One of the most important controversial point in the above article is the use of Fetal Bovine Serum (FBS) as a supplement of culture medium in their article. It is well documented that the FBS contains a high concentrations of nanoparticles, microvesicles, unknown extra cellular particle, proteins, growth factors, and unknown components. Therefore, isolation of exosomes from the extract derived from human umbilical cord-MSCs may be related to FBS components and not MSCs extract.

In accordance with our results, Wei *et al* in 2020 isolated nanoparticles from the human amniotic epithelial cells that propagated in a medium containing high-glucose DMEM (33 *mmol/l* glucose) supplemented with 10% FBS and 2% penicillin/streptomycin at 37°*C*, 5% CO_2, and 80% humidity. Similar to our protocol, when cell confluence reached 70-80%, the cells incubated with DMEM containing 10% exosome-free FBS for 48 *hr* and centrifuged for extraction of nanoparticle from supernatant. In this study, the nanoparticles extracted from the above protocol were presented a cup shape (spherical morphology) with a mean diameter of 105.89±10.36 *nm* that expressed the CD9, CD63, TSG101, and Alix molecular markers. Application of these nanoparticles in treating of diabetic ulcers significantly promoted cell proliferation, enhanced the migration of fibroblasts, suppressed the production of cytokines associated with inflammation, and facilitated

the angiogenic activity of cells. These researchers confirmed the biological effects of nanoparticles derived from amniotic epithelial cells on diabetic wound healing [18].

In 2024, Misaghian *et al* investigated the effect of nanoparticles derived from human Wharton's jelly-MSCs that were treated by polyinosinic-polycytidylic acid sodium salt on regulatory T cells. Then, the peripheral blood mononuclear cells were co-cultured with isolated nanoparticles for 6 days. In this study, the nanoparticles derived from treated Wharton's jelly-MSCs had an average size of 50 to 200 *nm*, with the most frequency of 132 *nm*. They confirmed that the 93% of purified nanoparticles had spherical morphology with an efficient integrated membrane and a diameter <132 *nm*. The exosomes derived from treated Wharton's jelly-MSCs significantly increased the frequency of CD4+CD25+Foxp3+egulatory T cells [19]. Dang *et al* also found that the nanoparticles derived from human umbilical cord-MSCs had a near-spherical shape with average size of 127.7 *nm*. These small size microvesicles were positive for CD63 and CD81 molecular markers [20].

In present study, nanoparticles with a higher negative zeta potential (-61.8 *mV*) indicate greater electrostatic stability (0.000481 cm^2/Vs) and reduced aggregation risk. To determine the stability of extracted nanoparticles in biological contexts, detection of zeta potential and electrostatic stability are necessary. These techniques can predict the colloidal behavior and tendency of nanoparticles for aggregation or agglomeration. The nanoparticles with a higher negative zeta potential (more negative surface charge) exhibit greater electrostatic stability and have a lower tendency to aggregation and agglomeration. However, a positive Zeta potential (less negative charge) indicates a greater chance for disruption and agglomeration, which potentially leads to adverse biological reactions and decreased therapeutic effectiveness.

Conclusion

Nanoparticles secreted from AD-MSCs, are considered promising therapeutic tools in tissue engineering and regenerative medicine. Nucleoproteins in the extracted nanoparticles in the experimental group was approximately 4 times higher than in the control group, which may indicate a greater therapeutic potential of these nanoparticles.

Ethical Approval

The study was approved by the Research Ethics Committee of the Islamic Azad University, Science and Research Unit, Tehran (IR.IAU.SRB.REC.1403.082).

Acknowledgement

The authors would like to thank the Yara Institute for technical support, ACECR, Tehran, and Dr. Kamali for assistance with the statistical analysis.

Conflict of Interest

The authors declared no conflict of interest.

References

1. Cai Y, Li J, Jia C, He Y, Deng, C. Therapeutic applications of adipose cell-free derivatives: a review. Stem Cell Res Ther 2020;11(1):312.
2. Barreca MM, Cancemi P, Geraci F. Mesenchymal and induced pluripotent stem cells-derived extracellular vesicles: the new frontier for regenerative medicine? Cells 2020;9(5):1163.
3. Chen B, Li Q, Zhao B, Wang Y. Stem cell-derived extracellular vesicles as a novel potential therapeutic tool for tissue repair. Stem Cells Transl Med 2017;6(9):1753-8.
4. Baglio SR, Rooijers K, Koppers-Lalic D, Verweij FJ, Pérez Lanzón M, Zini N, et al. Human bone marrow-and adipose-mesenchymal stem cells secrete exosomes enriched in distinctive miRNA and tRNA species. Stem Cell Res Ther 2015;6(1):127.
5. Kalluri R, LeBleu VS. The biology, function, and biomedical applications of exosomes. Science 2020;367 (6478):eaau6977.
6. Kiyota T, Machhi J, Lu Y, Dyavarshetty B, Nemati M, Yokoyama I, et al. Granulocyte-macrophage colony-stimulating factor neuroprotective activities in Alzheimer's disease mice. J Neuroimmunol 2018;319:80-92.
7. Dittmer J, Leyh B. Paracrine effects of stem cells in wound healing and cancer progression. Int J Oncol 2017; 44(6):1789-98.
8. Gao Y, Yuan Z, Yuan X, Wan Z, Yu Y, Zhan Q, et al. Bioinspired porous microspheres for sustained hypoxic exosomes release and vascularized bone regeneration. Bioact Mater 2022;14:377-88.
9. Gurunathan S, Kang MH, Jeyaraj M, Qasim M, Kim JH. Review of the isolation, characterization, biological function, and multifarious therapeutic approaches of exosomes. Cells 2019;8(4):307.
10. Zhang J, Walsh MF, Wu G, Edmonson MN, Gruber TA, Easton J, et al. Germline mutations in predisposition genes in pediatric cancer. N Engl J Med 2015;373(24): 2336-46.
11. Nam G-H, Choi Y, Kim GB, Kim S, Kim SA, Kim I-S. Emerging prospects of exosomes for cancer treatment: from conventional therapy to immunotherapy. Adv Mater 2020;32(51):2002440.
12. Vu NB, Nguyen HT, Palumbo R, Pellicano R, Fagoonee S, Pham PV. Stem cell-derived exosomes for wound healing: current status and promising directions. Minerva Med 2021;112(3):384-400.
13. Zhang Y, Jiayao B, Huang J, Tang Y, Du Sh, Pengyue L. Exosome: A review of its classification, isolation, storage, diagnostic and targeted therapy applications. Int J Nanomedicine 2020;15:6917-34.

14. Heidari B, Jaffary H, Golshahi H, Soltanghoraei H, Shams S, Soltani A, et al. Efficient procedure for human adipose tissue cryopreservation without specialized freezing equipment. Cryoletters 2025;46(3):197-206.
15. Heidari B, Eidi N, Mortazavi P, Saffarian Z, Soltani A, Mansouri P, et al. Morphological characteristics, mitochondrial oxidoreductase activity, and vascularization of human adipose tissues pre-and post-xenotransplantation into BALB/c female nude mice. Cryobiology 2025; 2025 May 6;119:105248.
16. Safwani WKZW, Wong CW, Yong KW, Choi JR, Adenan NAM, Omar S, et al. The effects of hypoxia and serum-free conditions on the stemness properties of human adipose-derived stem cells. Cytotechnology 2016;68 (5):1859.
17. Kim JY, Rhim WK, Seo HJ, Lee JY, Park CG, Han DK. Comparative analysis of MSC-derived exosomes depending on cell culture media for regenerative bioactivity. Tissue Eng Regen Med 2021;18(3):355-67.
18. Wei Q, Wei L, Zhang J, Li Z, Feng H, Ren L. EphA2-enriched exosomes promote cell migration and are a potential diagnostic serum marker in pancreatic cancer. Mol Med Rep 2020;22(4):2941-7.
19. Misaghian A, Ghadiri AA, Asadirad A, Amirzadeh S, Amari A. The Effect of Exosomes Isolated from Poly (I:C) Treated Human Wharton's Jelly Mesenchymal Stem Cells on CD4+CD25+Foxp3+Regulatory T Cells. Iran J Allergy Asthma Immunol 2024;23(3):288-98.
20. Dong B, Wang C, Zhang J, Zhang J, Gu Y, Guo X, et al. Exosomes from human umbilical cord mesenchymal stem cells attenuate the inflammation of severe steroid-resistant asthma by reshaping macrophage polarization. Stem Cell Res Ther 2021;12(1):204.